FERMILAB-PUB-20-119-TD
ACCEPTED
DOI: 10.1109/TASC.2020.2973119

Preload characterization of short models of MQXF the Nb_3Sn Low-β Quadrupole for the Hi-Lumi LHC

E. Takala, G. Ambrosio, N. Bourcey, D. W. Cheng, P. Ferracin, M. Guinchard, S. Izquierdo Bermudez, F. Mangiarotti, H. Pan, J.C. Perez, S. Prestemon, G. Vallone, T. Strauss

***Abstract*—MQXF is the Nb_3Sn Low-β Quadrupole magnet that the HL-LHC project is planning to install in the LHC interaction regions in 2026 as part of an upgrade to increase the LHC integrated luminosity by about a factor of ten. The magnet will be fabricated in two different lengths: 4.2 m for MQXFA, built in the US by the Accelerator Upgrade Project (AUP), and 7.15 m for MQXFB, fabricated by CERN. In order to qualify the magnet design and characterize its performance with different conductors, cable geometries and pre-load configuration, five short model magnets, called MQXFS, were fabricated, assembled and tested. The latest model, MQXFS6, uses a new powder-in-tube (PIT) superconducting wire, featuring a bundle barrier surrounding the filaments. The coil and the support structure were equipped with strain gauges and optical fibres to monitor strain during assembly, cool-down and excitation. In this paper we further develop the conventional azimuthal preload analysis and introduce a new set of tools for MQXF coil pack characterization which we use to analyse the behaviour of MQXFS6 room temperature preload and to reanalyse all the short models tested at CERN. A comparison is made between all the studied magnets revealing new characterizing preload parameters.**

***Index Terms*—Superconducting magnets, Nb3Sn wire, strain measurement, stress measurement**

I. Introduction

THE LHC is heading towards the HL-LHC upgrade [1] in which a new magnet design, MQXF [2-6], is used among other components in order to increase the luminosity by factor of two in the interaction points. The MQXF is designed to generate a nominal gradient of 132.6 T/m (aperture of 150 mm) having a peak field of 11.4 T. There are two types of end product, MQXFA and MQXFB produced respectively by the US Accelerator Upgrade Project (AUP, a continuation of LARP [7]) and by CERN. These magnets are 4.2 and 7.15 m long. A sequence of short models (MQXFS1/3/4/5 [8-10]) have been produced for testing purposes in order to fully understand the MQXF design, cross-section shown in Fig. 1. The preload of MQXF relies on the bladder and key technology. Approximately half of the required azimuthal coil compression is applied at room temperature by inserting loading keys in between the iron masters, thus pressing collars against coils. The other half of the compression is gained during the cool down as the aluminum shell shrinks more than the inner structure, thus further compressing the coils. Mechanically, one of the key parameters is the clearance between neighboring collars and the pole key. On one hand the pole key ensures the coil-collar alignment, however, on the other hand it intercepts the collars from effectively compressing the coil [9]. In this paper the continuation of the short model sequence, the MQXFS6, is introduced and its mechanical properties are discussed together with the earlier short models produced at CERN (MQXFS3/4/5). At the time of writing, the MQXFS6 has been assembled with powder-in-tube (PIT) coils, fully tested, disassembled, two of the coils exhibiting premature quench behavior changed (replacements from MQXFS5) and preloaded again. Mechanical changes in a magnet are differentiated with lower case suffixes, *e. g.* MQXFS6a/b. In this paper the focus is on the azimuthal preloading that is analyzed in section II with the help of shimming plans, transfer functions and so-called *key plots*. In section III, a non-matching coil-collar interface is analyzed with a help of a modified MQXF 2D finite element (FE) reference model [8-10].

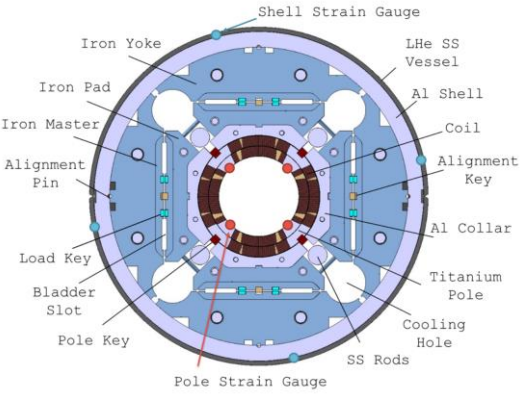

Fig. 1. The MQXF cross-section.

This work was supported by the U.S. Department of Energy, Office of Science, Office of High Energy Physics, through the US LHC Accelerator Research Program (LARP) and the US LHC Accelerator Upgrade Project (AUP), and by the High Luminosity LHC project at CERN.

E. Takala, N. Bourcey, P. Ferracin, M. Guinchard, S. Izquierdo Bermudez, F. Mangiarotti, J.C. Perez are with CERN, CH-1211 Geneva 23, Switzerland (e-mail: eelis.tapani.takala@cern.ch).

G. Ambrosio, T. Strauss are with Fermi National Accelerator Laboratory, Batavia, IL 80510 USA.

D. W. Cheng, H. Pan, S. Prestemon, G. Vallone, are with Lawrence Berkeley National Lab, Berkeley, CA 94720, USA

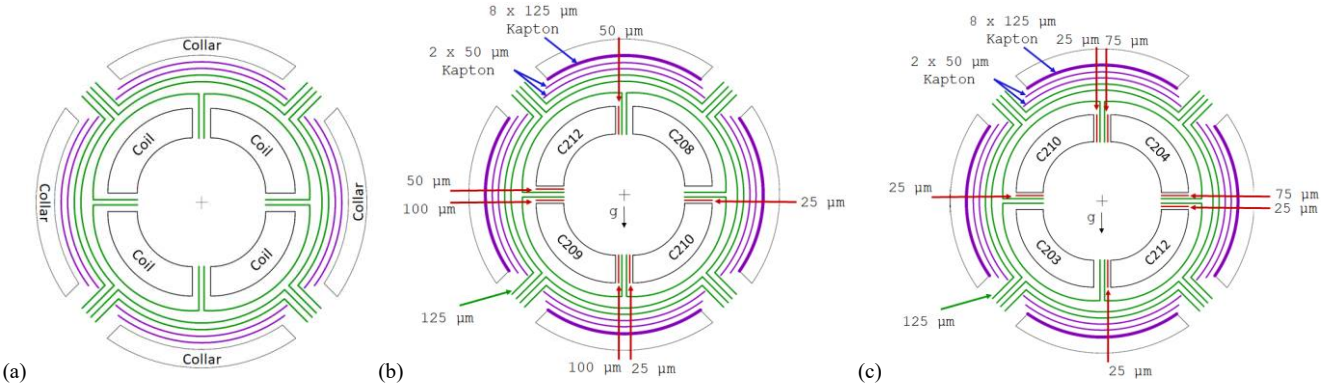

Fig. 2. Schematic view of the MQXF shimming plan (a) The nominal: coils wrapped with ground insulation (GI, 125 μm, green color), two collar matching GI layers, two additional shimming layers (125 μm, violet color) and collars with 114 mm inner radius; (b) MQXFS6a shimming plan (collar inner radius 115 mm); (c) MQXFS6b shimming plan (collar inner radius 115 mm)

TABLE I
PRELOAD SUMMARY FOR MQXF SHORT MODELS[1]

	MQXFS3 a/b	MQXF S5	MQXF S3c	MQXF S4	MQXF S6a	MQXF S6b
Coil cylinder (μm)[2]	95	63	63	-63	32	32
Radial shimming (μm) [2]	-200	-175	-200	-200	-150	-150
Coil pack plan (μm) [2]	-105	-112	-137	-263	-118	-118
Pole key clearance (μm) [3]	-50	50	200	100	300	npk
Shell stress (MPa) [4]	84	104	101	59	67	64
Coil stress (MPa) [4]	-75	-101	-116	-76	-83	-93
Axial force (MN)	0.23/0.71	0.58	0.69	0.67	0.72	0.67
Shell slope (MPa/mm)	124	128	122	123	112	128
Pole slope (MPa/mm)	-99	-152	-163	-205	-134	-209
TF slope (MPa/MPa)	-0.80	-1.2	-1.3	-1.7	-1.2	-1.6
Shell contact key (mm)	13.15	13.22	13.30	13.38	13.11	13.34
Pole contact key (mm)	13.25	13.25	13.36	13.41	13.11	13.38
Difference (μm) [5]	-100	-30	-60	-30	0[7]	-40
Coil pack meas. (μm) [5,6]	-150	-220	-300	-380	-110	-340
Coil pack diff. (μm) [8]	-45	-108	-113	-117	8	-222
Mechanical structure	D3	D3	D2	D3	D2	D2

[1]The models tested at CERN are listed in chronological order, [2]Radial size w.r.t. nominal, [3]npk means no pole key, [4]Azimuthal stress, [5]In terms of contact keys, [6]Radial size w.r.t. nominal shell contact keys, [7]fading offset, [8]The difference of measured and planned

II. PRELOADING

A. Shimming plan

In the MQXF design the coils are housed by the surrounding collars (Fig. 1). Free space is designed in between the touching parts in the housing. In order to guarantee conformal fitting, the free space is filled with shims that can be adjusted according to the real part sizes. Moreover, the space is used for fitting the ground insulation layers. A shimming plan shows how the free space in between the parts are filled. Fig. 2 shows the nominal and the final shimming plans of MQXFS6a/b. Note that there are two mechanical structures called MQXFSD2 (D2) and MQXFSD3 (D3), with thick vs. thin iron laminates [8]. In D2 the nominal inner collar radius is 115 mm and in D3 it is 114 mm. This difference is compensated with eight 125 μm Kapton layers. The difference w.r.t. the nominal in radial shimming and in coil cylinder radius is -150 μm and 32 μm, respectively. Thus the difference to nominal in coil pack [11] size is -118 μm. By convention [12] the shimming is left about 125 μm thinner in order to improve the coil-collar contact (see section III). A FUJI film test suggested that the contact is adequate.

Table I shows a comparison between the different MQXF short models. In MQXFS4 that has the shortest training and effective pressure transfer from shell to coil [10], the notable differences to the previous magnets are smallest coil cylinder and coil pack. Note that a large pole key clearance is also ensured. The clearance is also present in MQXFS3c, however the coils were previously heavily used (MQXFS3a/b). In MQXFS6 the objective is to ensure large enough clearance and final preload values similar to MQXFS4, which is more or less achieved.

B. Azimuthal preload

The azimuthal preload is applied by increasing the loading key size step by step [4]. The keys of all four quadrants of the magnet are changed one at the time. The azimuthal stress in the shell and the coils is usually recorded after all the sides are done (however the measurement system logs raw data every second for later analysis). The shell and coil stresses are defined as the average of the four gauges (see Fig. 1 for the positioning of the strain gauges). This procedure is repeated until the coil stress is at its target, taking into account the following creep. The recorded stress values are represented in a transfer function (TF) that describes the relationship between the shell and coil azimuthal stresses [8-10]. The measured TF can be compared with mechanical FE models. The MQXF design has 2D octant reference models to compare with the experimental results of short models and prototypes [8-10]. Usually the model is used to produce the pole key (pk) and no pole key (npk) lines that are the two extreme cases between which the measured TF should land, preferably tending towards the npk case [8-10].

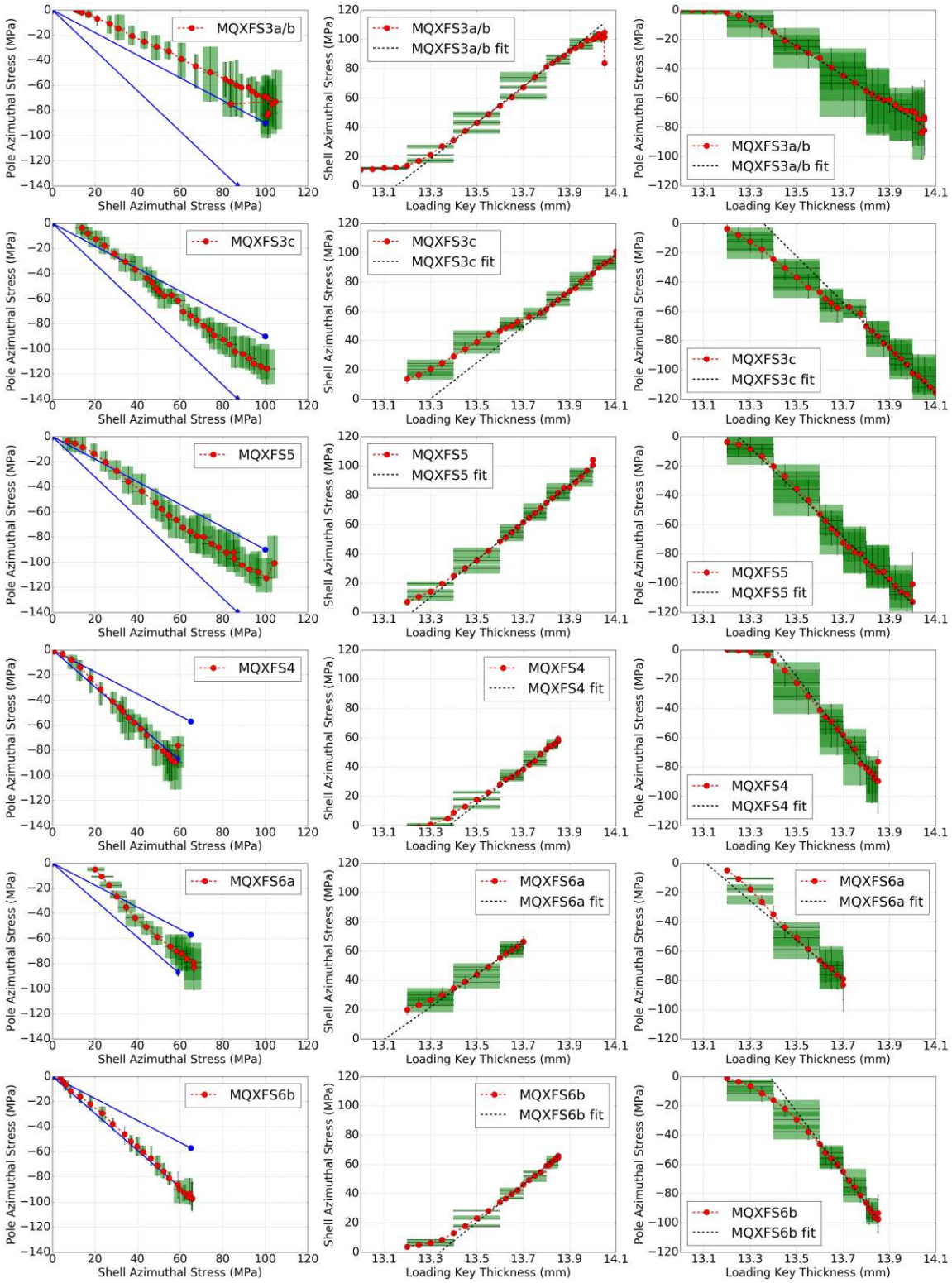

Fig. 3. Columns from left to right: the room temperature refined TF, the shell KP and the pole KP for different magnets. The last points of the curves are the creep values after loading (except in MQXFS3a/b where it is the preload value of "b" that only had an increase in axial preload with respect to "a"). The red circles are the measured averages and the green rectangles with black lines are the errors (the largest and lowest gauge values). The blue curves in the TF are the pole key (upper) and no pole key (lower) lines. The black dashed line is a linear fit.

C. *Analysis using refined TF and KPs*

Instead of recording the stress values at each full loading key cycle, the values can be recorded after each quadrant. On one hand the resulting refined TF includes mixed loading key states and thus the stress states are not all symmetric. On the other hand there are four times more data (thus the resulting plots are

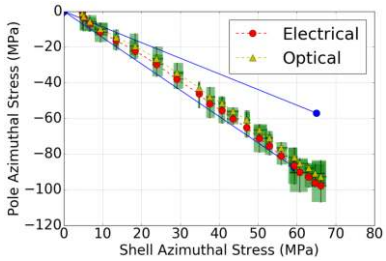

Fig. 4. A comparison of the refined TF curve of MQXFS6b with optical and electrical strain measurement systems.

called refined). The shell and the pole stresses can also be studied separately by relating the stress with the loading key size in a so-called key plot (KP).

The TF, the shell KP and the pole KP are shown in Fig. 3. A comparison of optical fibre and electrical strain gauge data is shown in Fig 4. The fibre data, that is in a good agreement with the electrical strain gauges but not available for all the magnets, is not used in this comparative preload study. The raw strain gauge data of the studied MQXFS magnets are reanalyzed using the refined data. The key size is computed as the average of all the keys. The refined TF seems to behave well: the mixed states land in between the full states in terms of shell and pole stresses. MQXFS3a/b is the only one for which adequate pole key clearance is not ensured, and indeed, the TF is above the pk line [8-10].

In regard to the KPs, the azimuthal preload consists of roughly two physical regimes: 1. The *loose regime*, where the parts are not yet in contact and the key size is increased little by little (see Fig. 1), the iron pads push the collars towards the coil and the yoke towards the shell until the parts are in contact (the procedure is called centering), 2. The *contact regime*, where further key increments lead to iron pads compressing the pole through the collars and iron yoke tensioning the shell.

The shell and the pole KPs should, in theory, both be piecewise linear functions with two parts: 1. starting at zero and staying flat until the nominal contact key size, then changing to 2. a positive (shell slope, $k_s>0$) or a negative (pole slope, $k_p<0$) slope in case of the shell and the pole, respectively. The contact key is the size of the smallest key that is required for a contact that generates a reaction to the shell (shell contact key, t_s) or the pole (pole contact key, t_p). Optimally, the shell and the pole would see the contact at the same time ($t_s = t_p$). If the pole compression is intercepted, *e. g.* in case of a large pole key, then $t_s < t_p$. The contact key difference is $t_d = t_s - t_p$. The coil pack size w.r.t. nominal in terms of contact key is defined as the difference of shell contact key and the nominal contact key (13 mm). The slope of the contact regime curve represents the rigidity in terms of stress vs loading key displacement ([MPa/mm]). Note that the TF slope is k_p/k_s. The linearity follows from three assumptions: 1. the materials are linear (in the first approximation), 2. the geometric deformation is very small and 3. the contacts are exhibiting linear behavior.

As seen in Fig. 3 the transition from the loose to the contact regime is in practice non-linear. This can be due to contact self-adjustments (parts never fit perfectly, *e. g.* the LQ effect [12]) during the transition. Moreover, the deeper contact regime may also be non-linear, possibly due to material non-linearity. This kind of behavior is observed only in MQXFS3a/b, where the shell KP shows decreased rigidity. It could be a sign of non-linear pole key deformation which would increase the pole key clearance and could explain the shift to the pk line in the TF [10] after the MQXFS3a thermo-cycle. In fact, an inspection after disassembly revealed a broken pole key. In MQXFS3c a slope change in both KPs at 13.75 mm is observed that could be attributed to a collar-pole key contact (would increase stiffness of the system).

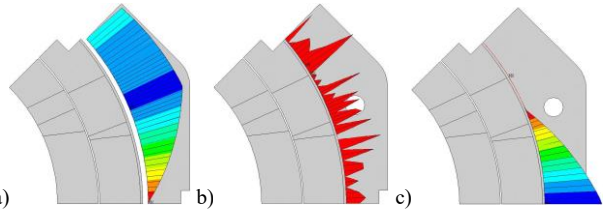

Fig. 5. MQXF coil and collar with the different profiles: a) *bump*, b) *nominal* and c) *dent* for studying the LQ effect on MQXF. The color scale from blue to red means 50 μm to 0 μm gap between coil pack and collar.

Based on an Ansys 3D model [13] the theoretical slopes for the no pole key and pole key cases, respectively, are 120 MPa/mm and 140 MPa/mm for the shell and -200 MPa/mm and -130 MPa/mm for the pole. The corresponding theoretical TF slopes are then -1.7 MPa/MPa and -0.9 MPa/MPa. The shell and pole stresses, axial force, slope and contact key results for each magnet are summarized in table I.

The TF slope shows that clearance is ensured in all the magnets except MQXFS3a/b where also the contact key difference is the highest. This is a strong indication of the lack of pole key clearance. Some contact key difference is seen in MQXFS3c and MQXFS5. Only in MQXFS6a the TF has a large offset that fades down after 30 MPa shell stress. This phenomenon is also seen in the KPs and hints at large pole bending (due to oversize or incompatible coil-collar interface, explained in the next section). Based on the pure slope numbers MQXFS6b is notably the ideal case of the npk case and indeed it is the first magnet assembled without a pole key. Moreover, MQXFS4 is very close to the npk case. Notably, MQXFS4 and MQXFS6b have the smallest coil pack sizes which in terms of contact keys are not only smaller than the nominal but also smaller than the expected sizes derived from the shimming plan, consistent within around 50 μm -100 μm (all, except MQXFS6a/b with 8/-222 μm). Note that the coil pack size in terms of contact keys depends on the fitting range: high shell stress may lead to irreversible coil deformation whereas shimming plan yields a theoretical non-deformed coil pack estimate. Moreover, the manufacturing tolerances of all the parts in the system play a role in this number.

III. The LQ effect on MQXF

Sometimes it might happen that the coil cylinder curvature is not compatible with that of the collar. This is referred to as the LQ effect [12]. It was studied with the help of a 2D Ansys model in the LQ magnet that had larger coil cylinder than expected. A similar study is be repeated for the MQXF with different coil curvature profiles.

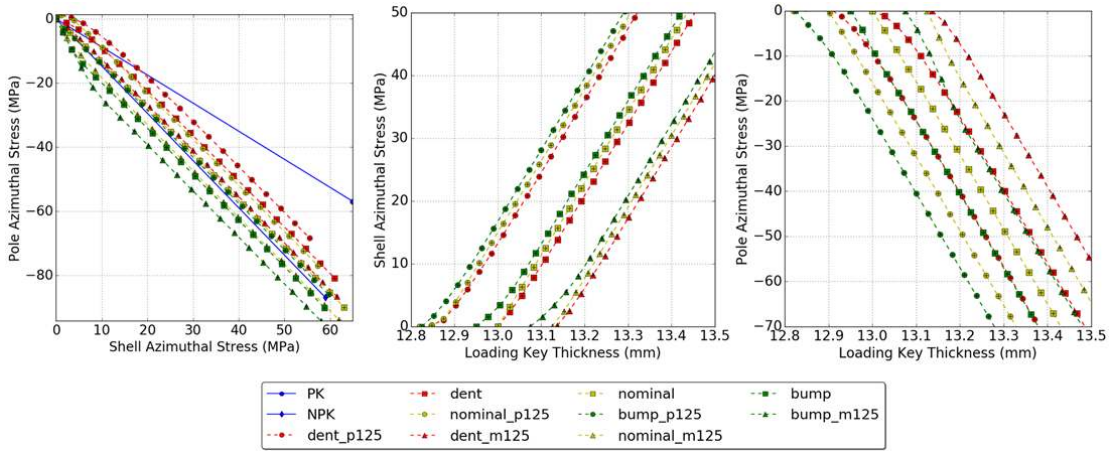

Fig. 6. The LQ effect on MQXFS4: TF, shell KP and Pole KP. The curves in the legend are in the same order (top to bottom, left to right) as they vertically appear in the TF plot. Note that the curve colors and markers are assigned for profile and modification groups as follows: red ~ dent, yellow ~ nominal, green ~ bump; circle ~ p125, square ~ , triangle ~ m125.

The reference 2D Ansys model for MQXF is used and the coil curvature profile is implemented with contact elements having variable gap size. The reference model is a symmetric octant and thus the gap size is defined as a function of the angle over the whole computation domain [0, 45]°. Let us define three basic profiles: 1. bump, 2. nominal and 3. dent. The bump is a 50 μm radial oversize starting on the mid plane (at 0°) linearly decreasing to 0 μm at 22.5° and the dent is the opposite of that (see Fig. 5). In real life the profiles could be compensated only by removing or adding shimming. This is studied in each case by removing or adding 125 μm shims (represented by m125 and p125 suffixes). The TFs and KPs based on these profiles are shown in Fig. 6.

The TFs show that having a bump or a dent on the mid-plane offsets the transfer function by a negative or a positive constant, respectively. This is due to the bending of the pole that takes place before the contact adjustment settles. In case there is a dent on the mid-plane, one should remove shims (m125) rather than add (p125) in order to compensate for the offset and vice versa for the bump (p125 rather than m125). Note that a dent or a bump of 50 μm can be compensated with the removal or addition, respectively, of a 125 μm shim.

In table II the contact key variation is shown for the different coil to collar profile features (the variation is read from Fig. 6 KPs). According to these results, shell contact key is less sensitive to mid-plane profile than the pole contact key. Thus it is more reliable for determining the coil pack size. Moreover, a 50 μm dent or bump will be seen as ∓ 35 μm contact key difference. Removing or adding 125 μm will be seen as ± 25 μm difference. The contact key difference in table I (other than MQXFS3a/b) could be explained by a bigger coil or a dent on the mid-plane. However, the coil packs are all smaller than nominal which suggest a dent on the mid-plane. MQXFS3a/b coil pack difference is affected by the -50 μm pole key clearance as it should decrease the shell contact key by the same amount (affecting contact key difference and coil pack difference).

TABLE II
CONTACT KEY VARIATION W.R.T. NOMINAL IN DIFFERENT COIL TO COLLAR CONTACT PROFILES FEATURES

Profile	m125	p125	dent	bump
Δt_s (μm)	125	-125	15	-15
Δt_v (μm)	100	-100	50	-50
Δt_d (μm)	25	-25	-35	35

IV. CONCLUSIONS

The MQXFS6 magnet is preloaded, tested, disassembled and preloaded again with two spare coils from MQXFS5. The shimming is performed in accordance with the conventional procedures, removing a 125 μm radial shim from the nominal. The preload targets are those of MQXFS4 (shortest training, no pole key preloading and a small contact key difference observed). The final values are in the neighborhood of the targets. A refined TF procedure and KPs are introduced for a deeper preload analysis. The reanalysis of all the studied MQXFS magnets with refined TF-KPs is done. A sign of a non-linear pole key deformation is found in MQXFS3a/b, moreover, inspection after tests showed a broken key. A slope change is observed in MQXFS3c KP, possibly due to a pole key contact. Contact key difference in MQXFS/3a/3b/3c/5 and a large fading down difference in MQXFS6a, suggests to a non-matching coil-collar interface which motivates the LQ effect study on MQXF. The study shows that a dent on the mid-plane or radial coil oversize can lead to the corresponding contact key difference. Moreover, it turns out that the coil pack size can be reliably defined with shell contact keys even when a small mid-plane dent or bump is present. Purely based on the LQ effect on MQXF and refined TF-KP analysis, it can be said that the MQXFS coil packs may suffer from radially undersized mid-planes (dent on the mid-plane). For a 50 μm dent, it is advised to remove 125 μm of radial shims; and as shown in MQXFS4 and MQXFS6b, it seems that the smaller coil pack is beneficial in reaching the optimal no pole key case.

REFERENCES

[1] "The High Luminosity Large Hadron Collider", edited by O. Brüning and L. Rossi, *World Scientific*, October 2015.

[2] E. Todesco, *et al.,* "Design Studies for the Low-Beta Quadrupoles for the LHC Luminosity Upgrade," *IEEE Trans. Appl. Supercond.*, vol. 23 no. 3, pp. 4002405, June 2013.

[3] E. Todesco, *et al.,* "A first baseline for the magnets in the high luminosity LHC insertion regions," *IEEE Trans. Appl. Supercond.*, vol. 24 no. 3, pp. 4003305, June 2014.

[4] P. Ferracin, *et al.,* "Magnet Design of the 150 mm Aperture Low-β Quadrupoles for the High Luminosity LHC," *IEEE Trans. Appl. Supercond.*, vol. 24 no. 3, pp. 4002306, June 2014.

[5] P. Ferracin, *et al.,* "Development of MQXF: The Nb_3Sn Low-β Quadrupole for the HiLumi LHC", *IEEE Trans. Appl. Supercond.*, vol. 26 no. 4, pp. 4000207, June 2016.

[6] E. Todesco, *et al.,* "Progress on HL-LHC Nb3Sn Magnets", *IEEE Trans. Appl. Supercond.,* vol. 28 no. 4, pp. 4008809, June 2018.

[7] S. A. Gourlay, *et al.*, "Magnet R&D for the US LHC Accelerator Research Program", *IEEE Trans. Appl. Supercond.*, vol. 16, no. 2, pp. 324-327, June 2006.

[8] G. Vallone, *et al.*, "Mechanical Performance of Short Models for MQXF, the Nb_3Sn Low-β Quadrupole for the Hi-Lumi LHC", *IEEE Trans. Appl. Supercond.*, vol. 27 no. 4, pp. 4002906, June 2017.

[9] G. Vallone, *et al.*, "Mechanical Analysis of the Short Model Magnets for the Nb_3Sn Low-β Quadrupole MQXF", *IEEE Trans. Appl. Supercond.*, vol. 28 no. 3, pp. 4003106, April 2018.

[10] G. Vallone, *et al.*, "Summary of the Mechanical Performances of the 1.5 Long Models of the Nb_3Sn Low-β Quadrupole MQXF", *IEEE Trans. Appl. Supercond.*, vol. 29 no. 5, pp 4002805

[11] P. Ferracin, *et al.,* , "Development of MQXF: The Nb_3Sn Low-β Quadrupole for the HiLumi LHC", *IEEE Trans. Appl. Supercond.*, vol. 26 no. 4, pp. 400207, June 2016

[12] P. Ferracin, *et al.*, "Mechanical Performance of the LARP NbSn Quadrupole Magnet LQS0", *IEEE Trans. Appl. Supercond.*, vol. 21 no. 3, pp. 1683, June 2011

[13] M. Juchno, et al., "Support Structure Design of the Nb_3Sn Quadrupole for the High Luminosity LHC", *IEEE Trans. Appl. Supercond.*, vol. 25, no. 3, June 2015